SCIENTIFIC REPORTS

OPEN

SUBJECT AREAS:
SENSORS AND BIOSENSORS
NEMS
MAGNETIC DEVICES
NANOSENSORS

Received
4 April 2013

Accepted
28 May 2013

Published
13 June 2013

Correspondence and requests for materials should be addressed to M.R. (rinaldi@ece.neu.edu) or N.S. (nian@ece.neu.edu)

* These authors contributed equally to this work.

Self-Biased 215MHz Magnetoelectric NEMS Resonator for Ultra-Sensitive DC Magnetic Field Detection

Tianxiang Nan*, Yu Hui*, Matteo Rinaldi & Nian X. Sun

Department of Electrical and Computer Engineering, Northeastern University, Boston, MA 02115, USA.

High sensitivity magnetoelectric sensors with their electromechanical resonance frequencies $<$ 200 kHz have been recently demonstrated using magnetostrictive/piezoelectric magnetoelectric heterostructures. In this work, we demonstrate a novel magnetoelectric nano-electromechanical systems (NEMS) resonator with an electromechanical resonance frequency of 215 MHz based on an AlN/(FeGaB/Al_2O_3) × 10 magnetoelectric heterostructure for detecting DC magnetic fields. This magnetoelectric NEMS resonator showed a high quality factor of 735, and strong magnetoelectric coupling with a large voltage tunable sensitivity. The admittance of the magnetoelectric NEMS resonator was very sensitive to DC magnetic fields at its electromechanical resonance, which led to a new detection mechanism for ultra-sensitive self-biased RF NEMS magnetoelectric sensor with a low limit of detection of DC magnetic fields of ~300 picoTelsa. The magnetic/piezoelectric heterostructure based RF NEMS magnetoelectric sensor is compact, power efficient and readily integrated with CMOS technology, which represents a new class of ultra-sensitive magnetometers for DC and low frequency AC magnetic fields.

Strong magnetoelectric (ME) coupling has been demonstrated in magnetostrictive/piezoelectric magnetoelectric heterostructures[1–6], which has enabled different novel magnetoelectric devices, including magnetoelectric sensors[7–10], spintronics[11–14], voltage tunable microwave magnetoelectric devices[15–17], etc. Exciting progress has been made recently on magnetoelectric sensors, which are highly sensitive magnetometers based on magnetic control of electrical polarization in magnetic/piezoelectric magnetoelectric heterostructures[7,8,10,18]. In particular, these magnetoelectric sensors show over 1 ~ 2 orders of magnitude enhanced magnetoelectric coefficients and sensitivity when the AC excitation magnetic field frequency matches the electromechanical resonance of the laminates. A high magnetoelectric coefficient of 737 V/cm·Oe at the electromechanical resonance frequency of 753 Hz was demonstrated using FeCoSiB/AlN thin film magnetoelectric heterostructures at a bias magnetic field of 6 Oe[19]. An optimum DC bias magnetic field is required for magnetoelectric sensors to reach maximum magnetoelectric coupling coefficient and sensitivity, which results in additional source of noise and makes it hard for integration. Exchange bias has been most recently introduced in IrMn/FeCoSiB/AlN heterostructures to achieve magnetoelectric sensors with strong magnetoelectric coupling coefficient at zero bias magnetic field, which made possible self-biased thin film magnetoelectric sensors at the cost of a reduced magnetoelectric coupling coefficient compared to FeCoSiB/AlN bilayer[7,19].

It has been an open challenge in sensing weak DC and low frequencies AC magnetic fields. The DC magnetic field dependence of magnetoelectric coupling can be used for DC magnetic field sensing[20]. However, an AC magnetic field is needed for driving the magnetoelectric sensors at certain frequency for sensing DC magnetic field[20]. The large power consumption for generating AC magnetic fields and comparatively low sensitivity make it challenging in sensing DC magnetic fields for magnetoelectric sensors. Moreover, a significant amount of recent research effort has also been devoted to increasing the sensitivity for $<$ 10 Hz AC fields due to the large 1/f noise[21,22] in magnetoelectric sensors by lowering the electromechanical resonance frequency of magnetoelectric devices[23,24] or reducing the equivalent magnetic noise at low frequency[25]. However, further reducing the electromechanical resonance frequency of magnetoelectric sensors will lead to excessively large sensor sizes that would be impractical for real applications.

In this paper, we demonstrated a self-biased magnetoelectric sensor based on a 215 MHz AlN/(FeGaB/Al_2O_3) × 10 magnetoelectric NEMS nano-plate resonator with a highly piezomagnetic and low loss FeGaB/Al_2O_3 multilayer[26]. Different mechanism was used in the NEMS magnetoelectric sensor by measuring the DC magnetic field dependence of the admittance of the magnetoelectric NEMS nano-plate resonator, of which the DC

magnetic field sensitivity is linearly proportional to the resonance frequency. By increasing the resonance frequency of the NEMS magnetoelectric sensor to 215 MHz, a low limit of detection for DC magnetic fields of ~300 picoTesla in unshielded environment was achieved. A comparable limit of detection at zero bias magnetic field was also observed, which enables a self-biased magnetoelectric sensor without bias DC magnetic fields and AC excitation magnetic fields for detecting DC and low frequency AC magnetic fields. This novel ultra-miniaturized self-biased NEMS magnetoelectric sensor working at 215 MHz with ultra-high sensitivity can be readily integrated with CMOS technology, which constitutes a new class of compact and ultra-sensitive integrated RF NEMS magnetometers.

Results

The NEMS magnetic field sensor with a DC magnetic field applied on the length direction of the sensor is shown in Figures 1(a), (b) and (c). The AlN/($FeGaB/Al_2O_3$) × 10 magnetoelectric heterostructure has seven Pt inter-digital electrodes on the bottom of the AlN layer and highly piezomagnetic low-loss RF ($FeGaB/Al_2O_3$) × 10 multilayer as the electrically floating top electrode. The pitch W_0 of the Pt inter-digital electrodes was set to be 11 μm which induced a extensional mode of vibration in AlN layer with a very high electromechanical resonance frequency of 215 MHz. The sensing area fully covered by the magnetic materials was 100 μm (W) × 200 μm (L) as displayed by the scanning electron microscopy image of the NEMS magnetic field sensor in Figure 1(c). Figure 1(d) shows the cross section image of the RF NEMS magnetoelectric sensor, indicating a 250 nm thick AlN piezoelectric layer, a 250 nm thick ($FeGaB/Al_2O_3$) × 10 multilayer, and a 50 nm thick Pt bottom electrode with a flat and tight interface between the three layers which could lead to a high magnetoelectric coupling. The complete removal of Si substrate underneath the RF NEMS resonator, by diminishing substrate clamping effect, also results to a strong magnetoelectric coupling and high sensitivity[10].

The admittance curve and the Butterworth–van Dyke (BVD) model fitting of the NEMS magnetic field sensor are depicted in Figure 2(a) showing an electromechanical resonance frequency of 215 MHz. A high quality factor of 735 in air was extracted from the BVD fitting at zero bias magnetic field, while the quality factors reported in different magnetoelectric sensors devices operating at low frequencies were around 100[10,27]. The ($FeGaB/Al_2O_3$) × 10 multilayer electrically floating electrode provides good confinement of the electric field within the entire thickness of AlN layer, which results in a high electromechanical coupling coefficient k_t^2 of 1.54%, comparable to what is typically achieved in conventional AlN nano-plate resonator employing the same electrode configuration[28].

Strong magnetoelectric coupling in the AlN/($FeGaB/Al_2O_3$) × 10 based RF NEMS resonator was demonstrated in a DC bias field induced change in the electromechanical resonance frequency, which was attributable to the bias magnetic field induced Young's modulus change in FeGaB, or the delta-E effect[29]. Figure 2(c) shows the admittance curve of the NEMS magnetic field sensor at various DC bias magnetic fields (0 Oe, 15 Oe and 60 Oe) applied along the length direction of the resonator. Both resonance frequency *f*, and peak admittance amplitude *Y*, at the resonance frequency collected in Figure 2(d) exhibited a similar trend with DC bias magnetic field, which first decreased with the increase of bias field, reaching minimum values at a bias field of 15 Oe, and then increased until the ($FeGaB/Al_2O_3$) × 10 multilayer was saturated at 50 ~ 60 Oe. From the BVD fitting results, the quality factor (Q) followed the similar trace that the Q started from 735 (0 Oe) then reached the minimum value of 250 at the transition magnetic field (15 Oe) and finally saturated to 1400 at high magnetic fields (> 60 Oe). The variation of the Q can be attributed to the magnetic loss associated with magnetic domain wall activities which were significantly reduced when high magnetic field was applied and the magnetic domain wall was eliminated.

The resonance frequency of the magnetoelectric NEMS resonator can be expressed by

$$f_0 = \frac{1}{2W_0}\sqrt{\frac{E_{eq}}{\rho_{eq}}}, \tag{1}$$

with W_0 being the pitch of the finger electrodes forming the inter-digital transducer (IDT), E_{eq} the equivalent Young's Modulus and ρ_{eq} the equivalent density of the resonator. A magnetostrictive strain can be induced in the FeGaB layer under a DC magnetic field through the delta-E effect, which led to a changed Young's modulus of the FeGaB film, and therefore a changed equivalent Young's modulus of

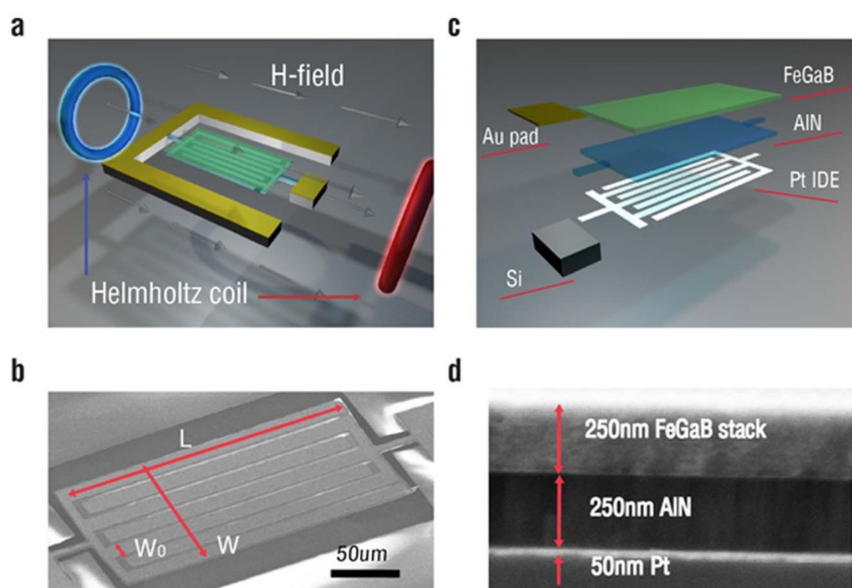

Figure 1 | (a) Schematic of the NEMS magnetic field sensor. The DC magnetic field was applied on the length direction of the sensor. (b) Scanning Electron Microscopy (SEM) images of the fabricated NEMS magnetic field sensor. (c) Schematic of the layered structure of the NEMS magnetic field sensor. (d) Scanning Electron Microscopy (SEM) image of cross section of the NEMS sensor.

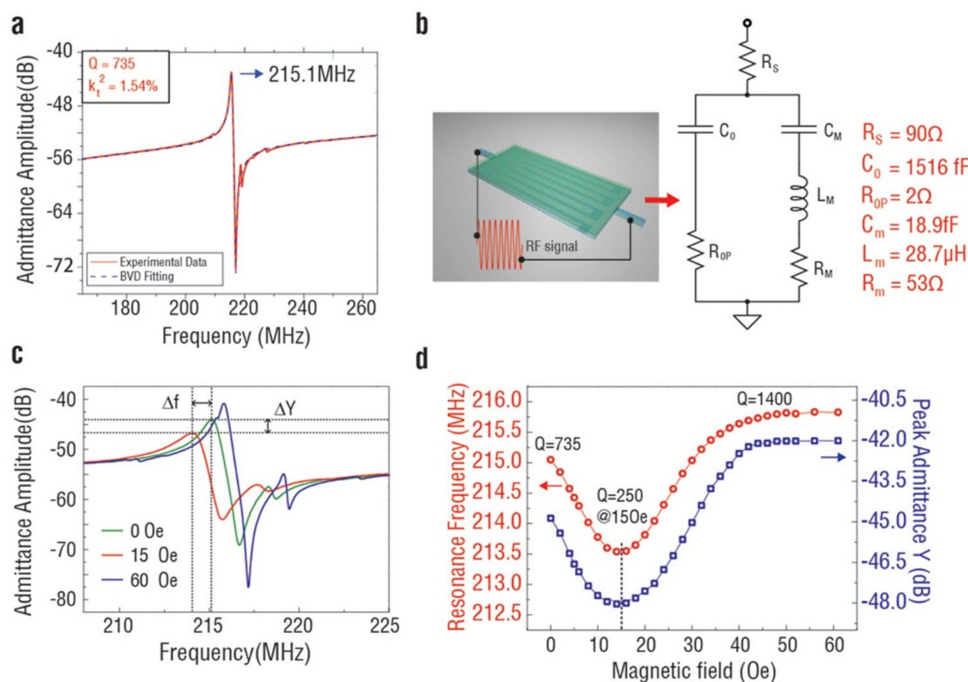

Figure 2 | (a) Admittance curve and Butterworth–van Dyke (BVD) model fitting of the fabricated NEMS magnetic field sensor. (b) The BVD equivalent electrical circuit of the resonator, in which R_s is the resistance of metal electrodes and contact resistance, R_{op} is the parasitic resistance from substrate, C_0 is the device capacitance from the Pt/AlN/FeGaB stack, C_M, L_M and R_M are the motional capacitance, inductance and resistance, respectively. (c) Admittance curve of the NEMS sensor at various bias DC magnetic fields. (d) Resonance frequency and admittance amplitude at the resonance frequency as a function of DC magnetic field.

the NEMS magnetoelectric resonator. Thus the electromechanical resonance frequency and the admittance amplitude of the AlN resonator were varied through DC magnetic fields. The admittance amplitude at the resonance frequency has a similar trend to resonance frequency change due to the variation of the Q and f_0. The lowest resonance frequency of the device happened when the bias magnetic field was around 15 Oe which is close to the bias field needed for reaching the highest piezomagnetic coefficient of the FeGaB[26].

An extremely small magnetic field was applied to the NEMS sensor to measure the sensitivity to DC magnetic fields in a magnetically and electrically unshielded lab environment. Figure 3 shows the admittance amplitude of the magnetoelectric sensor starting from 50pTesla bias magnetic field by exciting the RF NEMS magnetoelectric resonator at one single frequency between the series and parallel resonances where the slope of admittance amplitude versus frequency reaches the maximum[30]. In order to get the highest sensitivity, an extremely small DC magnetic field to be measured was superimposed to a fixed DC bias magnetic field (5 Oe) for tuning the magnetic materials to reach the maximum slope of electromechanical resonance frequency versus magnetic field. Figure 3 inset shows the zoomed in area with the small DC magnetic field ranging from 50pT to 4nT. The measurement value of the admittance amplitude starts to scatter at 300 picoTelsla, indicating the ultra-sensitive magnetic sensor with a detection range starting from ~300 picoTesla.

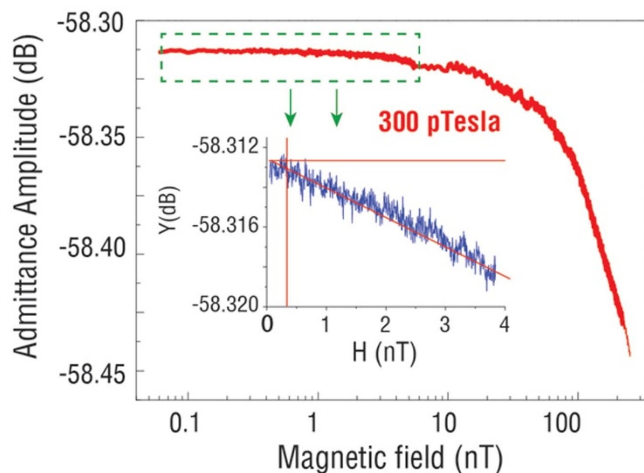

Figure 3 | **The sensitivity and linearity of the magnetic field sensor, showing the admittance amplitude as a function of a minute varied DC bias magnetic field superimposed a fixed DC field of 5 Oe.** The inset shows the zoomed in part ranging from 50pTesla to 4nTesla in a magnetically unshielded environment.

The magnetic field dependence of the admittance of the same 215 MHz magnetoelectric NEMS resonator is shown in Figure 4 at zero bias magnetic field, showing a limit of detection as low as 600 picoTesla under self-bias condition comparable to a limit of detection of 300 picoTelsla at an optimum bias field of 5 Oe. The magnetoelectric coupling coefficient is linearly proportional to the piezomagnetic coefficient, which is highly dependent upon the DC bias magnetic field. The piezomagnetic coefficient is close to zero at zero bias magnetic field for most magnetic materials, which lead to a zero or very low magnetoelectric coupling coefficient of the magnetoelectric sensors without DC bias magnetic fields. An optimal DC bias magnetic field is therefore required for achieving maximum piezomagnetic coefficient and sensitivity for magnetoelectric sensors. Compared to conventional magnetoelectric sensors that rely on the magnetoelectric voltage output for measuring AC magnetic fields and need a bias magnetic field for operation, our demonstrated RF NEMS magnetoelectric sensors are based on the magnetic field dependence of admittance of the NEMS resonator, which makes them excellent self-biased magnetometers.

Strong converse magnetoelectric coupling in the AlN/(FeGaB/Al_2O_3) × 10 based RF NEMS resonator was achieved through

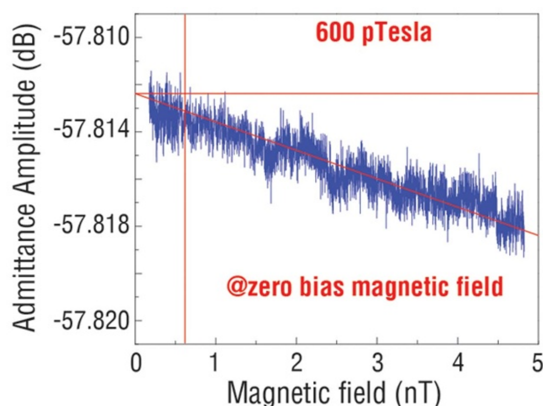

Figure 4 | The sensitivity and linearity of the magnetic field sensor at zero bias magnetic field in a magnetically unshielded environment.

electric field induced effective magnetic field. An applied DC voltage on the AlN layer led to a piezoelectric strain in the AlN and in FeGaB, which resulted in a strain induced effective magnetic field in FeGaB layer. Tunability of the RF NEMS resonance frequency and the transition magnetic field (the magnetic field H at the minimum resonance frequency) which is 15 Oe at zero bias DC voltage was achieved by applying different DC voltages superimposed to the RF signal via a bias Tee on the piezoelectric AlN layer, as showed in Figure 5. The resonance frequency of the magnetoelectric RF NEMS resonator at zero magnetic field was tuned by an applied DC voltage. A positive DC voltage led to enhanced resonance frequency of the NEMS resonator; while a negative DC voltage resulted in decreased resonance frequency, which can be attributed to the change of the stiffness of the resonator by the induced piezoelectric stress[31]. As the DC voltage was applied on the inter-digital electrodes of the AlN layer, a DC in-plane stress was induced due to the piezoelectric effect by the vertical component of the electric field.

When the piezoelectric strain in AlN was transferred to the magnetic materials, an effective anisotropy field H_{eff} would be induced which can be expressed as $H_{eff} = -\frac{3\lambda\sigma}{M_s}$, where σ is the in-plane stress transferred from piezoelectric AlN layer to magnetostrictive FeGaB layer; λ is the in-plane magnetostriction coefficient for magnetic phase; M_s is the saturation magnetization[32]. The applied positive voltage induced a positive H_{eff} along the width direction while the negative voltage induced a negative H_{eff}, which alters the transition field collected in the Figure 5 inset. Essentially, the magnetic anisotropy field H_K which determines the required external magnetic field for maximum piezomagnetic coefficient is changed by the effective magnetic field induced by the applied voltage on AlN layer. The linear relationship between the magnetic transition fields and the applied voltages results from the linear piezoelectricity of AlN, indicating a strong converse magnetoelectric coupling between the piezomagnetic phase and the piezoelectric phase. The tunability of the transition field can be calculated as the fraction of variation of the transition magnetic field (ΔH) to the transition magnetic field (H_0) at zero bias magnetic field expressed as $\Delta H/H_0 = 13\%$. The linear region below the transition magnetic field could be defined as the DC magnetic field measurement range of the magnetoelectric sensor, the applied DC voltage is able to tune the detecting range as well as the sensitivity (the slope of the resonance frequency to magnetic field) to the magnetic field in the range. The applied negative DC voltage made the sensor more sensitive with a narrow detecting range while the positive voltage expanded the detecting range with lower sensitivity. The large tunability of the device shows the feasibility in different DC magnetic field sensing application with distinct detecting range and sensitivity.

Discussion

RF Micro/Nano-Electro-Mechanical Systems (MEMS/NEMS) resonators have been widely used for different sensors based on its impedance or resonance frequency change. The ultra-miniaturized RF MEMS device with CMOS compatible technology working at very high frequency may provide much potential of application in highly sensitive, low power consumption compact magnetometers. The limit of detection of the magnetoelectric NEMS sensors is expected to be linearly proportional to the operation frequency.

The measured admittance sensitivity of the sensor to DC magnetic field in Figure 3 and 4 can be expressed as

$$\frac{dY}{dH} = \frac{dY}{df}\frac{df}{dH} = \frac{dY}{df}\left(\frac{df}{dE}\frac{dE}{dH} - \nu\frac{df}{dW}\frac{dW}{dH}\right), \quad (2)$$

where Y is the admittance amplitude, E is the Young's modulus of the resonator, ν is the Poisson's ratio of the magnetic materials, W is the width of the inter-digital electrodes. The $\frac{dY}{df}$ term is the slope of admittance amplitude versus frequency between series and parallel resonances where the slope reaches the maximum; while $\frac{df}{dH}$ can be seen as the resonance frequency sensitivity to the DC magnetic fields. The shift of the frequency due to magnetostrictive strain is negligible comparing with ΔE effect, since the magnetostriction coefficient of FeGaB of 70 ppm is much smaller than the delta-E effect induced percentage change in Young's modulus of magnetostrictive soft magnetic films which can be up to 20% ~30%[29]. The slope of the res-

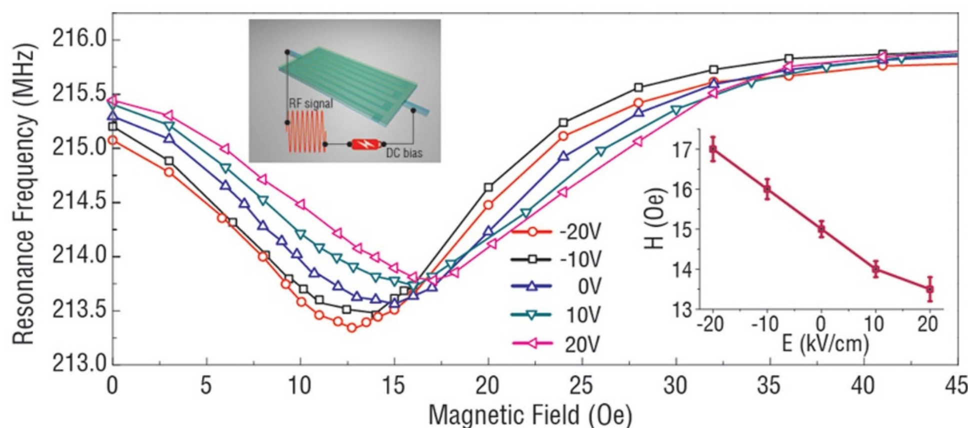

Figure 5 | Electromechanical resonance frequency of the magnetoelectric RF MEMS resonator as a function of DC magnetic fields under different DC electric fields applied to the AlN layer. The inset shows the magnetic fields H at the minimum resonance frequency versus the applied electric fields.

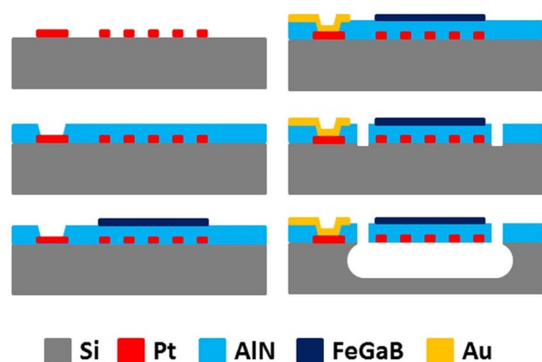

Figure 6 | Fabrication process of NEMS magnetic field sensor.

onance frequency as a function of DC magnetic field curve [figure 2 (d)] depicts the $\frac{df}{dH}$, which was comparably high at zero DC magnetic field. Unlike the piezomagnetic coefficient which is almost zero at zero bias magnetic field, the change of Young's modulus due to magnetic domain wall motion is not zero at zero bias magnetic field, which makes the NEMS magnetoelectric sensor a self-biased device. Moreover the frequency sensitivity can be simplified from equation (2) and substituted by equation (1) as

$$\frac{df}{dH} = \frac{df}{dE}\frac{dE}{dH} = \frac{f}{2E}\frac{dE}{dH}, \tag{3}$$

clearly, the higher resonance frequency of the sensor would results in higher sensitivity $\left(\frac{df}{dH}\right)$ to the magnetic field. The 215 MHz resonant NEMS sensor was fabricated to reach high sensitivity due to the sensitivity to frequency relation.

Such unprecedented demonstrations are enabled by the combination of the extraordinary transduction properties, at nanoscale, of the AlN Nano Plate Resonator (NPR) technology[33–35]. The efficient on-chip piezoelectric actuation and sensing of a high frequency bulk acoustic mode of vibration in a nano-plate structure enables the fabrication of a 215 MHz frequency resonator with efficient transduction. Converse magnetoelectric coupling is also achieved in the NEMS sensor to modify the sensitivity and detecting range via electric field. The nano-scale, self-biased and CMOS compatible fabrication process make the NEMS magnetoelectric sensor high-potential in application of real magnetic sensor device. The NEMS magnetoelectric sensors with up to GHz range will be demonstrated in the near future which are expected to acquire much lower limit of detection for magnetic fields.

Method

Fabrication process. The NEMS magnetic field sensor of this work was fabricated using a five-mask microfabrication process, shown in Figure 6. A high resistivity Silicon (Si) wafer (> 10000 ohm·cm) was used as substrate. A 50 nm thick Platinum (Pt) film was sputter-deposited and patterned by lift-off on top of the Si substrate to define the bottom IDT. Then, the 250 nm thick AlN film (stress 60 MPa and FWHM 2.2°) was sputter-deposited and vias to access the bottom IDT electrode were etched by H_3PO_4. Next, the 250 nm thick FeGaB/Al_2O_3 multilayer layer was deposited by Physical Vapor Deposition (PVD) and patterned by lift-off. A 20 Oe in-situ magnetic field bias was applied during the PVD deposition along the width, W, of the device to pre-orient the magnetic domains. Then, a 50 nm thick gold (Au) film was evaporated and patterned by lift-off to form the top electrode. After that, the AlN film was etched by Inductively Coupled Plasma (ICP) etching in Cl_2 based chemistry to define the shape of the resonant nano-plate. Finally, the structure was released by XeF_2 isotropic etching of the Silicon substrate.

Admittance curve measurement. The on-chip NEMS magnetic field sensor was measured by a network analyzer (Agilent PNA 8350b) connecting to the electrode pads by RF probes. The transmission parameter S_{11} was acquired and converted to admittance amplitude. The available power at the network analyzer port was set to -12 dBm, and the IF bandwidth was 200 Hz which results to a trace noise magnitude of 0.002 dB. The magnetic field was applied along the width direction during the measurements.

Sensitivity measurement. The device was excited at one frequency between the series and parallel resonances where the slope of admittance amplitude versus frequency reaches the maximum. The extreme small DC magnetic field was applied along the length direction of the device by a home-made Helmholtz coil driven by a precision current source Keithley 6220.

1. Spaldin, N. & Fiebig, M. The Renaissance of Magnetoelectric Multiferroics. *Science* **309**, 391–392 (2005).
2. Eerenstein, W., Mathur, N. D. & Scott, J. F. Multiferroic and magnetoelectric materials. *Nature* **442**, 759–765 (2006).
3. Fiebig, M. Revival of the magnetoelectric effect. *Journal of Physics D: Applied Physics* **38**, R123–R152 (2005).
4. Martin, L. W. *et al.* Multiferroics and magnetoelectrics: thin films and nanostructures. *Journal of Physics: Condensed Matter* **20**, 434220 (2008).
5. Nan, C. W., Bichurin, M. I., Dong, S., Viehland, D. & Srinivasan, G. Multiferroic magnetoelectric composites: Historical perspective, status, and future directions. *Journal of Applied Physics* **103**, 031101 (2008).
6. Sun, N. X. & Srinivasan, G. Voltage Control of Magnetism in Multiferroic Heterostructures and Devices. *Spin* **02**, 1240004 (2012).
7. Lage, E., Kirchhof, C., Hrkac, V., Kienle, L., Jahns, R., Knöchel, R., Quant, E. & Meyners, D. Exchange biasing of magnetoelectric composites. *Nature Materials* **11**, 523–529 (2012).
8. Israel, C., Mathur, N. D. & Scott, J. F. A one-cent room-temperature magnetoelectric sensor. *Nature Materials* **7**, 93–94 (2008).
9. Zhai, J., Xing, Z., Dong, S., Li, J. & Viehland, D. Detection of pico-Tesla magnetic fields using magneto-electric sensors at room temperature. *Applied Physics Letters* **88**, 062510 (2006).
10. Zhao, P. *et al.* Fabrication and characterization of all-thin-film magnetoelectric sensors. *Applied Physics Letters* **94**, 243507 (2009).
11. Nan, T. X. *et al.* Voltage impulse induced bistable magnetization switching in multiferroic heterostructures. *Applied Physics Letters* **100**, 132409 (2012).
12. Hu, J. M., Li, Z., Chen, L. Q. & Nan, C.-W. High-density magnetoresistive random access memory operating at ultralow voltage at room temperature. *Nature Communications* **2**, 553 (2011).
13. Tsymbal, E. Y. Spintronics: Electric toggling of magnets. *Nature Materials* **11**, 12–13, doi:10.1038/nmat3205 (2011).
14. Wu, T. *et al.* Electrical control of reversible and permanent magnetization reorientation for magnetoelectric memory devices. *Applied Physics Letters* **98**, 262504 (2011).
15. Ustinov, A. B., Srinivasan, G. & Kalinikos, B. A. Ferrite-ferroelectric hybrid wave phase shifters. *Applied Physics Letters* **90**, 031913 (2007).
16. Liu, M., Lou, J., Li, S. & Sun, N. X. E-Field Control of Exchange Bias and Deterministic Magnetization Switching in AFM/FM/FE Multiferroic Heterostructures. *Advanced Functional Materials* **21**, 2593–2598 (2011).
17. Das, J., Song, Y.-Y., Mo, N., Krivosik, P. & Patton, C. E. Electric-Field-Tunable Low Loss Multiferroic Ferrimagnetic-Ferroelectric Heterostructures. *Advanced Materials* **21**, 2045–2049 (2009).
18. Dong, S., Cheng, J., Li, J. F. & Viehland, D. Enhanced magnetoelectric effects in laminate composites of Terfenol-D/Pb(Zr,Ti)O_3 under resonant drive. *Applied Physics Letters* **83**, 4812 (2003).
19. Greve, H., Woltermann, E., Quenzer, H. J., Wagner, B. & Quandt, E. Giant magnetoelectric coefficients in $(Fe_{90}Co_{10})_{78}Si_{12}B_{10}$-AlN thin film composites. *Applied Physics Letters* **96**, 182501 (2010).
20. Dong, S., Zhai, J., Li, J. & Viehland, D. Small dc magnetic field response of magnetoelectric laminate composites. *Applied Physics Letters* **88**, 082907 (2006).
21. Edelstein, A. S. & Fischer, G. A. Minimizing 1/f noise in magnetic sensors using a microelectromechanical system flux concentrator. *Journal of Applied Physics* **91**, 7795 (2002).
22. Stutzke, N. A., Russek, S. E., Pappas, D. P. & Tondra, M. Low-frequency noise measurements on commercial magnetoresistive magnetic field sensors. *Journal of Applied Physics* **97**, 10Q107 (2005).
23. Dong, S., Zhai, J., Xing, Z., Li, J. F. & Viehland, D. Extremely low frequency response of magnetoelectric multilayer composites. *Applied Physics Letters* **86**, 102901 (2005).
24. Greve, H. *et al.* Low damping resonant magnetoelectric sensors. *Applied Physics Letters* **97**, 152503 (2010).
25. Wang, Y. *et al.* An Extremely Low Equivalent Magnetic Noise Magnetoelectric Sensor. *Advanced Materials* **23**, 4111–4114 (2011).
26. Lou, J., Liu, M., Reed, D., Ren, Y. & Sun, N. X. Giant Electric Field Tuning of Magnetism in Novel Multiferroic FeGaB/Lead Zinc Niobate-Lead Titanate (PZN-PT) Heterostructures. *Advanced Materials* **21**, 4711–4715 (2009).
27. Marauska, S. *et al.* MEMS magnetic field sensor based on magnetoelectric composites. *Journal of Micromechanics and Microengineering* **22**, 065024 (2012).
28. Rinaldi, M., Zuo, C., Van der Spiegel, J. & Piazza, G. Reconfigurable CMOS Oscillator based on Multi-Frequency AlN Contour-Mode MEMS Resonators. *IEEE Transactions on Electron Devices* **58**, 1281–1286 (2010).

29. Ludwig, A. & Quandt, E. Optimization of the E Effect in Thin Films and Multilayers by Magnetic Field Annealing. *IEEE TRANSACTIONS ON MAGNETICS* **38**, 2829–2831 (2002).
30. Rinaldi, M., Zuniga, C. & Piazza, G. Ultra-Thin-Film AlN Contour-Mode Resonators for Sensing Applications. *Proceedings of the IEEE International Ultrasonics Symposium*, 714–717 (2009).
31. Karabalin, R. B. *et al.* Piezoelectric nanoelectromechanical resonators based on aluminum nitride thin films. *Applied Physics Letters* **95**, 103111 (2009).
32. Liu, M. *et al.* Electrical tuning of magnetism in Fe3O4/PZN–PT multiferroic heterostructures derived by reactive magnetron sputtering. *Journal of Applied Physics* **107**, 073916 (2010).
33. Rinaldi, M., Zuniga, C. & Piazza, G. 5-10 GHz AlN Contour-Mode Nanoelectromechanical Resonators. *Proceedings of the 22nd IEEE Conference on Micro Electro Mechanical Systems*, 916–919 (2009).
34. Rinaldi, M., Zuniga, C., Zuo, C. & Piazza, G. AlN Contour-Mode Resonators for Narrow-Band Filters above 3 GHz. *Proceedings of the IEEE International Frequency Control Symposium*, 70–74 (2009).
35. Rinaldi, M., Zuniga, C., Zuo, C. & Piazza, G. Super-High-Frequency Two-Port AlN contour mode resonators for RF applications. *IEEE Transactions on Ultrasonics, Ferroelectrics, and Frequency Control* **57**, 38–45 (2010).

Acknowledgements

This work is funded by AFRL through UES FA8650-090-D-5037, NSF CAREER Award ECCS-0746810 and ECCS-0824008, DARPA Young Faculty Award N66001-12-1-4221. We are grateful to X. Yang, Y. Gao, Z. Qian, Z. Zhou and M. Liu for their assistance. Also the authors wish to thank the staff of the George J. Kostas Nanoscale Technology and Manufacturing Research Center at Northeastern University where the device was fabricated.

Author contributions

Tianxiang Nan and Yu Hui contributed equally in this work with fabrication and testing of the devices. Nian Sun and Matteo Rinaldi initiated the original idea of the RF magnetoelectric NEMS resonator for magnetic field sensing. Tianxiang Nan prepared the main manuscript and all authors reviewed the manuscript.

Additional information

Competing financial interests: The authors declare no competing financial interests.

How to cite this article: Nan, T., Hui, Y., Rinaldi, M. & Sun, N. Self-Biased 215MHz Magnetoelectric NEMS Resonator for Ultra-Sensitive DC Magnetic Field Detection. *Sci. Rep.* **3**, 1985; DOI:10.1038/srep01985 (2013).

This work is licensed under a Creative Commons Attribution-NonCommercial-NoDerivs Works 3.0 Unported license. To view a copy of this license, visit http://creativecommons.org/licenses/by-nc-nd/3.0